Cement and Concrete Research 137 (2020) 106190

Contents lists available at ScienceDirect

Cement and Concrete Research

journal homepage: www.elsevier.com/locate/cemconres

Characterization of amorphous and crystalline ASR products formed in concrete aggregates

Andreas Leemann[a,*], Zhenguo Shi[a], Jan Lindgård[b]

[a] Empa, Swiss Federal Laboratories for Materials Science and Technology, Dübendorf, Switzerland
[b] SINTEF, Trondheim, Norway

ARTICLE INFO

Keywords:
Concrete
Alkali-silica reaction
Shlykovite
Microstructure
Composition

ABSTRACT

Amorphous and crystalline alkali silica reaction (ASR) products formed in aggregates of two different concrete mixtures exposed to the concrete prim test both at 38 °C and 60 °C have been analysed by scanning electron microscope with energy dispersive X-ray spectroscopy and by Raman microscopy. Additionally, amorphous ASR products were synthesized and analysed with Raman microscopy and ^{29}Si nuclear magnetic resonance. Amorphous ASR products display a higher Na/K-ratio than crystalline ones. Both types of products display a structure dominated by Q^3-sites (Si-tetrahedra with three bridging oxygen atoms typical for a layer structure) with a secondary amount of Q^2-sites (Si-tetrahedra with two bridging oxygen atoms typical for a chain structure). Temperature in the CPT alters the structure of the crystalline ASR. While the Raman spectra of the product formed at 38 °C is identical to the one formed in concrete structures, the one of the 60 °C product corresponds to K-shlykovite.

1. Introduction

Concrete damages due to alkali silica reaction (ASR) occur worldwide [1]. The expansion causing the damage is the result of the reaction between the alkaline pore solution in concrete and reactive SiO_2 in aggregates causing the subsequent formation of ASR products. In a recent study, the use of caesium as a tracer incorporated in ASR products has made it possible to follow the sequence of reaction down to the nanometre scale [2]. The first ASR products are formed in pre-existing pores of the aggregate close to the cement paste. With ongoing reaction, ASR products advance towards the interior of the aggregates. This ingress goes together with a simultaneous stress generation, eventually leading to aggregate cracking. Many of these newly formed cracks are not restricted to the aggregates and continue into the cement paste with the concurrent extrusion of ASR products. After the initial crack formation, the mostly empty cracks in the aggregates start to fill with ASR products, again advancing from the periphery of the aggregate towards the interior. In contrast to the initial phase of reaction, where the ASR products are amorphous, the second stage is characterized by the formation of primarily crystalline ASR products.

The chemical composition of the crystalline ASR products formed in aggregates was analysed in various studies [3–7]. However, only few data are available on the differences in the composition of amorphous and crystalline ASR products formed in aggregates. There have been several attempts to link the structure of the crystalline ASR product to existing minerals by comparison of XRD patterns or based on chemical composition [5,8–10]. Recently, attempts have been made to resolve the structure of the crystalline ASR products based on micro-XRD measurements of concrete samples performed in a synchrotron facility [11,12] and on powder-XRD of synthetic samples [13,14]. Additionally, Raman microscopy has been used to characterize these crystalline ASR products [13–16]. There are some indications that there are differences between the crystalline ASR products formed in structures and in the concrete prism test at 38 °C compared to the ones formed in the concrete prism test at 60 °C [13–15]. The latter is practically identical to synthesized K-shlykovite [13,14]. However, such observation was made on different concretes rather than on the same concrete mix design tested at both temperatures. Even less is known about the amorphous ASR products in this regard. There have been attempts to characterize the structure of amorphous ASR products using various methods [17–19]. However, these studies have the considerable drawback that the samples were not obtained from the interior of concrete aggregates. They were collected on the concrete surface of a dam, where they were in direct contact with the cement paste and additionally exposed to carbonation, which would likely alter their properties. A few Raman spectra of amorphous ASR products formed in aggregates of concrete from an ASR-affected structure were presented in Ref. [16]. A wider data set of amorphous ASR products present in aggregates and cement

* Corresponding author.
E-mail address: andreas.leemann@empa.ch (A. Leemann).

https://doi.org/10.1016/j.cemconres.2020.106190
Received 25 March 2020; Received in revised form 23 June 2020; Accepted 29 July 2020

paste of mortar bars immersed in KOH and NaOH at 80 °C was published in Ref. [20]. However, no direct connection between Raman spectra of the amorphous ASR products and their composition was presented, making it impossible to improve the understanding between structure and composition and differentiate the amorphous ASR products from calcium-silicate-hydrates (C-S-H).

The goal of this study is to improve the knowledge on ASR products formed in concrete aggregates by investigating:

- the differences in chemical composition between amorphous and crystalline ASR products;
- the variation in the chemical composition of crystalline ASR products formed in different aggregate particles of the same concrete;
- the structure of crystalline ASR products formed at 38 and 60 °C;
- the structure of amorphous ASR products.

To reach these goals, scanning-electron microscopy (SEM) combined with energy dispersive X-ray spectroscopy (EDS) and Raman microscopy are used to analyse ASR products formed in two different concrete mixtures both tested with the CPT at 38 and 60 °C. Additionally, Raman spectra are obtained from amorphous ASR products formed in aggregates of field-exposed concrete and from synthesized amorphous ASR products. Moreover, ^{29}Si nuclear magnetic resonance (^{29}Si MAS NMR) is performed on two samples of synthesized ASR products.

2. Materials and methods

2.1. Materials

Concrete C1 and C2 were produced with a cement content of 440 kg/m^3 and a w/c of 0.45. The Na_2O-equivalent of the cement was 1.26 mass-%. Cement composition is given in Table 1. For concrete C1, the aggregate used was a natural gravel with low reactivity, mainly consisting of granite and feldspatic rocks. The aggregate employed to produce concrete C2 was a medium reactive natural gravel, consisting of various rock types with about 25% of potential reactive rock types (sandstone, mylonite/cataclasite, siltstone/silt-claystone/meta-marl). Three prisms (100 × 100 × 450 mm^3) of both concrete mixtures were produced for the Norwegian concrete prism test at 38 °C [21] and three prisms (70 × 70 × 280 mm^3) for the concrete prism test at 60 °C [22]. The expansion determined in the tests and on field-exposed cubes (300 × 300 × 300 mm^3) are shown in Table 2. The field-exposed samples were not available for analysis, because they are still used to measure the ongoing expansion.

Samples of all concrete mixtures were cut after the CPT and locations of interest were identified. Areas close to the surface of the samples were discarded, as they may have been affected by alkali leaching [26] or carbonation. The samples for backscattering images SEM-imaging and EDS were dried for three days at 50 °C, impregnated with epoxy resin, polished and carbon coated.

Samples for Raman microscopy and SE-imaging in the SEM were separated from cut concrete sections using chisel and hammer. After isolating aggregates containing cracks with ASR products, they were split along these cracks. Samples for Raman were stored in a dry cabinet and samples for SEM were dried at 50 °C for a day and then carbon coated. Due to the small amount of ASR products present in concrete C1–38, it was not possible to perform a Raman analysis.

As concrete C1 and C2 stored outdoors (Table 2) were not available for analysis, two concrete mixtures containing silicate aggregates (C-S1 and C-N1) comparable the ones in concrete C1 and C2 were used to obtain Raman spectra of amorphous ASR products. The spectra were compare to the ones obtained in the samples tested with the CPT. Cubes produced with these concrete mixtures were stored for 13 years at an outdoor exposure site in Valencia within the framework of the PARTNER project [23]. Expansion data is given in Table 2.

Table 2
Expansion of the different concrete mixtures.

	CPT 38 °C	CPT 60 °C	Natural exposure
Concrete C1	C1–38: 0.12%/110 weeks	C1–60: 0.40%/155 weeks	0.01%/9 years[a] −0.01%/8 years[b]
Concrete C2	C2–38: 0.23%/110 weeks	C2–60: 0.29%/150 weeks	0.04%/9 years[a] 0.16%/8 years[b]
Concrete C-N1	0.32%/52 weeks[c]	0.20%/20 weeks[c]	0.68%/13 years[d]
Concrete C-S1	0.05%/52 weeks[c]	0.05%/20 weeks[c]	0.12%/13 years[d]

[a] Exposed at SINTEF's field exposure site in Trondheim, Norway.
[b] Exposed at LNEC's field exposure site in Lisbon, Portugal.
[c] Data from Ref. [23].
[d] Exposed at PARTNER field exposure site in Valencia, Spain. Data from Refs. [24,25].

Additionally, amorphous ASR products were synthesized by adding $Ca(OH)_2$ to saturated alkali silicate solution. The alkali silicate solution was produced by adding 90 g/l of silica gel (Fluka Silica Gel 40) to a 0.75 M solution of NaOH and KOH (molar Na/K-ratio = 1). Four different amounts of $Ca(OH)_2$ suspended in 5 ml of distilled water were added to 25 ml saturated alkali silicate solution under constant stirring at 20 °C. The stirring was stopped when gelation occurred. The samples were stored for three weeks at 20 °C before washing them with isopropanol to wash out excess alkalis. The samples were dried under vacuum 0.03 ± 0.01 mbar for 3 days. This drying technique prevents carbonation. Raman spectra were acquired immediately after drying. Additionally, XRD analysis showed that no crystalline phases were present in the synthetic gels (data not shown). An influence of carbonates on the Raman spectra can therefore be excluded.

In order to be able to link the Raman spectra of the amorphous products formed in aggregates to a specific chemical composition, analysis was performed by EDS at the location of spectra acquisition. EDS analysis on broken surfaces is influenced by surface roughness and inclination. Therefore, the composition of the amorphous products has to be regarded as indicative and therefore, only the ratios are given (Table 3). The composition of the synthetic gels was measured on impregnated and polished samples by EDS showing a Ca/Si-ratio of 0.07, 0.17, 0.27 and 0.33 for the four samples (Table 3).

2.2. Methods

For the analysis of the polished concrete samples a Nova NanoSEM 230 FEI was used. It was run in the high vacuum mode (3.0–5.0 × 10^{-6} Torr) with an acceleration voltage of 12 kV, a spot size of 4.5 and a beam current of 90–100 μA. An Qxford SSD detector (80 mm^2) and INCA Energy software with ZAF correction were used for the EDS analysis. All other samples were analysed with a FEI Quanta 650. An acceleration voltage of 8–12 kV, a spot size from 3.0–4.5 and a pressure of 3.0–5.0 × 10^{-6} Torr were applied depending on the detector used (back-scattering electron (BSE) or secondary electron (SE) detector). Chemical analysis was performed by energy-dispersive X-ray spectroscopy (EDS) with a Thermo Noran Ultra Dry 60 mm^2 detector

Table 1
Cement composition in mass-%.

	SiO_2	Al_2O_3	Fe_2O_3	MnO	TiO_2	P_2O_5	CaO	MgO	K_2O	Na_2O	SO_3	LOI	TC
CEM I 42.5	19.6	4.9	3.3	0.1	0.3	0.2	61.9	2.5	1.2	0.45	3.6	1.6	0.4

Table 3
Approximate ratios of the amorphous ASR products formed in concrete aggregates and synthesized amorphous ASR products analysed with Raman microscopy. "Distance to ITZ" refers to the distance between the surface of the aggregate to the location of Raman spectra acquisition in the aggregate.

Sample	Ca/Si	(Na + K)/Si	Na/K	Distance to ITZ [μm]
C2–38	0.29	0.40	0.62	180
C2–38	0.31	0.47	0.77	100
C-N1	0.30	0.36	0.74	150
C-S1	0.20	0.45	1.41	140
Syn-0.07	0.07	0.26	1.20	–
Syn-0.17	0.17	0.33	1.26	–
Syn-0.27	0.27	0.41	1.11	–
Syn-0.33	0.33	0.36	1.33	–

and Pathfinder X-Ray Microanalysis Software. For the polished samples, a BSE detector was used in combination with EDS and for the broken samples the SE detector was deployed to acquire images. About 2400 points were analysed with EDS in concrete C1 and C2. The elemental ratios given in the paper always refer to atomic percentages.

A Raman Bruker Senterra microscope was used for spectra acquisition. The laser wavelength was 532 nm, operating power 20 mW and lens magnification 50×. The instrument was equipped with a Peltier-cooled CCD detector and operated with Opus 6.5 software. 20–40 spectra with a resolution of 3–5 cm^{-1} were collected per sample. The spectra were baseline corrected, averaged and smoothed by a running mean of 11. The designation of the specific Raman bands is based on spectra published on alkali-silicates, historic glasses, silicate glasses and melts. These publications are listed in Refs. [13,16] with the most important ones being [27–32].

A Bruker AVANCE III NMR spectrometer was employed for ^{29}Si MAS NMR measurements using a 7 mm CP/MAS probe at 79.5 MHz. The same parameters as in Refs. [13,14] were applied. The ^{29}Si NMR chemical shifts were externally referenced to tetramethylsilane (TMS) at 0.0 ppm.

3. Results

3.1. ASR products formed in concrete

3.1.1. Allocation of amorphous and crystalline ASR products

ASR products are present as thin layers often reaching sub-micrometre thickness between adjacent mineral grains, as described in detail in Ref. [2]. In spite of the small volumes present, which limit the possibilities to analyse the products, the lack of texture indicates that they are amorphous. After crack formation, all concrete mixtures display the typical distribution of amorphous and crystalline products. The amorphous ASR products in the aggregates are typically present as a plug close to the interface and entirely fill the cracks. Additionally, they form thin linings with a thickness of a few micrometres along the crack walls that extend several hundred micrometres into the interior of the aggregates. Here, they typically occur together with crystalline ASR products that start to fill the cracks advancing from the periphery of the aggregate towards the interior (Fig. 1). Still the majority of the cracks in the aggregates are filled only in part with ASR products. In contrast to this situation, the cracks in the cement paste are usually completely filled with amorphous ASR products that have extruded the aggregates simultaneously to crack formation [2]. Some aggregates do not develop a major crack with a width of several tens of micrometres progressing into the cement paste, but they form multiple cracks with a width < 10 μm. As these cracks do not extend into the cement paste, the extruding amorphous ASR products fills pores in the interfacial transition zone. This situation appears to occur more frequently in the concrete tested at 60 °C compared to the one tested at 38 °C.

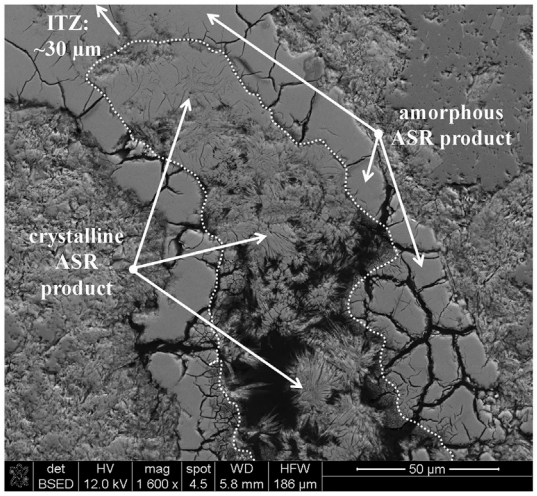

Fig. 1. Amorphous and crystalline ASR products in a cracked aggregate in concrete C1–60. Dotted line indicates boundary between amorphous and crystalline products. Interface to the cement paste at a distance of ~30 μm from upper left corner of image. HFW = 186 μm.

3.1.2. Chemical composition of ASR products

3.1.2.1. Differences in composition between amorphous and crystalline ASR products. A distinction has to be made between the amorphous ASR products present in the aggregates and the ones extruding into the cement paste. The former displays a Ca/Si-ratio of ~0.24 and a (Na + K)/Si-ratio of ~0.28 (Table 4). Other elements like Mg, Al and Fe are only present as traces. The ASR products in the cement paste on the other hand take up calcium, leading to an increased Ca/Si-ratio of > 0.4 [3–6,16]. The Ca uptake usually goes together with a decrease of the alkali content. The zone in a crack filled with these types of products, where such increase in Ca/Si ratio occurs, changes from aggregate to aggregate. Sometimes, the increase starts when the amorphous ASR product has progressed into the cement paste for 30–40 μm. Sometimes, the zone of increased Ca/Si-ratio already starts in the aggregates. However, the maximum depth (distance from the surface of the aggregate) of increased Ca/Si-ratio in the studied aggregates was never > 30 μm. For the comparison with the crystalline ASR products, only amorphous ASR products in the aggregates with a distance to their surface > 30 μm were taken into account.

The amorphous ASR products show a slightly larger variation in the Ca/Si-ratio than the crystalline one, with slightly higher average values (Table 4, Fig. 2). Additionally, their alkali content is higher compared to the crystalline ones. However, the most prominent difference is the Na/K-ratio, with considerably higher values for the amorphous products (Fig. 3).

3.1.2.2. Variations in the composition of crystalline ASR products. There is some variation in the composition of the crystalline ASR products formed in the different aggregate particles. These differences are easily visible in ratio-plots (Figs. 4 and 5). In concrete C1–38, Ca/Si-ratio and (Na + K)/Si of different aggregates vary between 0.19–0.25 and 0.18–0.27, respectively. While the variations are in an identical range for the (Na + K)/Si-ratio in concrete C1–60, the variation of the Ca/Si-ratio is smaller with 0.20–0.22. The same applies to the ASR products formed in the aggregate particles of concrete C2: identical variation in the (Na + K)-ratio and smaller variation of the Ca/Si-ratio in concrete C2–60. In both concrete mixtures the average values for the Ca/Si-ratio are slightly lower and the average (Na + K)/Si-ratio slightly higher at a testing temperature of 60°compared to 38 °C.

Table 4
Chemical composition of amorphous and crystalline ASR products formed in aggregates of the different concrete mixtures (am = amorphous, cry = crystalline). Mean values with standard deviations.

Samples	Type	O	Na	Mg	Al	Si	S	K	Ca	Fe	Ca/Si	(Na + K)/Si	Na/K
		[atom-%]									[−]		
C1–38	am	68.6	1.4	0.0	0.4	20.9	0.0	3.2	5.3	0.1	0.26	0.22	0.46
		± 2.0	*± 0.5*	*± 0.1*	*± 0.6*	*± 1.3*	*± 0.1*	*± 0.8*	*± 0.6*	*± 0.4*	*± 0.03*	*± 0.06*	*± 0.21*
	cry	69.5	0.8	0.0	0.2	21.2	0.0	3.6	4.5	0.0	0.21	0.21	0.27
		± 2.3	*± 0.7*	*± 0.1*	*± 0.3*	*± 1.8*	*± 0.1*	*± 0.9*	*± 0.7*	*± 0.3*	*± 0.03*	*± 0.05*	*± 0.25*
C1–60	am	69.0	2.8	0.0	0.0	19.4	0.0	3.7	4.5	0.5	0.23	0.34	0.76
		± 1.3	*± 0.6*	*± 0.1*	*± 0.1*	*± 0.7*	*± 0.1*	*± 0.4*	*± 0.8*	*± 0.3*	*± 0.04*	*± 0.04*	*± 0.13*
	cry	69.7	0.5	0.0	0.0	20.7	0.0	4.5	4.4	0.1	0.21	0.24	0.10
		± 2.4	*± 0.3*	*± 0.1*	*± 0.3*	*± 1.6*	*± 0.1*	*± 0.8*	*± 0.6*	*± 0.3*	*± 0.02*	*± 0.05*	*± 0.08*
C2–38	am	71.2	0.8	0.0	0.0	19.9	0.0	3.6	4.5	0.0	0.25	0.26	0.61
		± 2.0	*± 0.8*	*± 0.1*	*± 0.5*	*± 1.9*	*± 0.1*	*± 0.6*	*± 1.0*	*± 0.3*	*± 0.06*	*± 0.07*	*± 0.23*
	cry	71.2	0.8	0.0	0.0	19.9	0.0	3.6	4.5	0.0	0.23	0.22	0.22
		± 2.7	*± 0.4*	*± 0.1*	*± 0.2*	*± 1.8*	*± 0.1*	*± 0.7*	*± 0.7*	*± 0.3*	*± 0.03*	*± 0.04*	*± 0.11*
C2–60	am	69.8	2.0	0.0	0.1	19.9	0.0	3.4	4.3	0.3	0.22	0.28	0.71
		± 1.5	*± 1.2*	*± 0.2*	*± 0.3*	*± 1.5*	*± 0.1*	*± 1.0*	*± 0.7*	*± 0.5*	*± 0.04*	*± 0.05*	*± 0.47*
	cry	69.2	0.4	0.0	0.0	21.2	0.0	4.5	4.6	0.1	0.22	0.23	0.11
		± 2.3	*± 0.3*	*± 0.1*	*± 0.1*	*± 1.7*	*± 0.1*	*± 0.8*	*± 0.6*	*± 0.3*	*± 0.02*	*± 0.04*	*± 0.07*

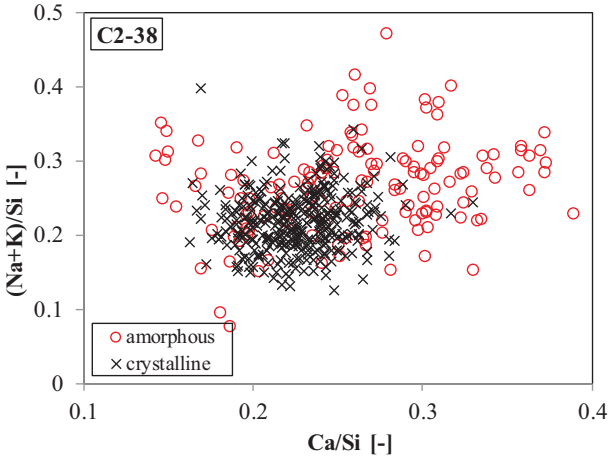

Fig. 2. (Na + K)/Si-ratio of amorphous and crystalline ASR products as a function of their Ca/Si-ratio.

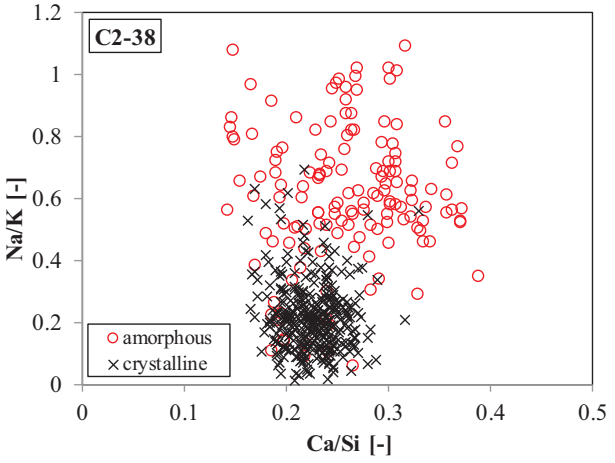

Fig. 3. Na/K-ratio of amorphous and crystalline ASR products as a function of their Ca/Si-ratio.

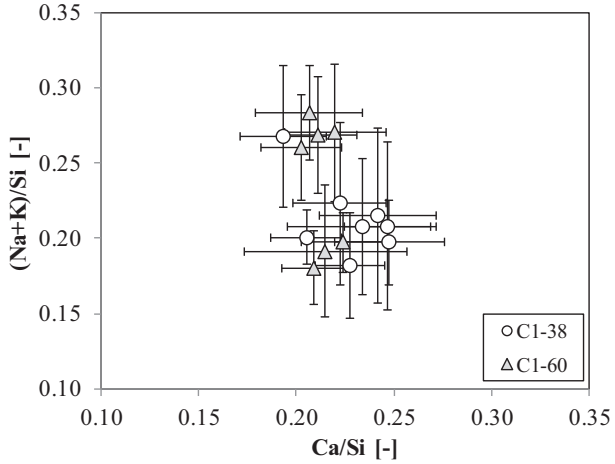

Fig. 4. (Na + K)/Si-ratio as a function of Ca/Si-ratio of crystalline ASR products formed in aggregate particles of concrete C1 tested at 38 and 60 °C. Mean values with standard deviations.

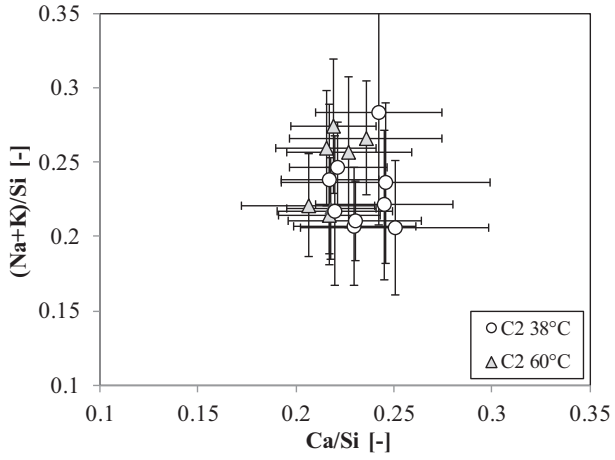

Fig. 5. (Na + K)/Si-ratio as a function of Ca/Si-ratio of crystalline ASR products formed in aggregate particles of concrete C2 tested at 38 and 60° C. Mean values with standard deviations.

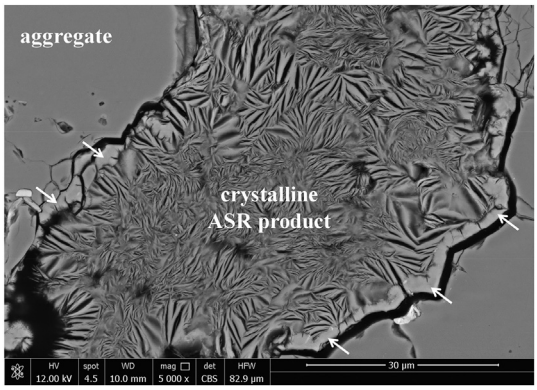

Fig. 6. Tightly packed crystalline ASR product formed in an aggregate particle of concrete C2–38. Note the thin layers of amorphous ASR products lining the crack walls (white arrows). Distance to the surface of the aggregate ≈ 2.0 mm. HFW = 83 µm.

3.1.3. Morphology of the crystalline ASR products

Usually, crystalline ASR products formed in aggregates are tightly packed (Fig. 6). The small gaps between the platy mineral bundles are the result of drying before epoxy impregnation. In some locations along the split aggregate particles, crystals were able to grow in space without restraint, thereby showing their idiomorphic form (Fig. 7). All the studied samples, including the one of a bridge used as reference, show thin platelets. The ones formed in the reference and in concrete C2–38 are isometric (Fig. 7A and C). The platelets formed in concrete C1–60 and C2–60 are more elongated (Fig. 7B and D).

3.1.4. Raman microscopy

3.1.4.1. Amorphous ASR products. No meaningful Raman spectra of amorphous ASR products were obtainable in concrete C1–38, C1–60 and C2–60. The measured spectra were always a mixture between signals of amorphous and crystalline ASR products, making the identification of the distinct bands of the amorphous products impossible. However, Raman spectra of amorphous ASR products in several aggregates of concrete C2–38 were obtained. All spectra were collected at a distance to the interface with the cement paste > 100 µm

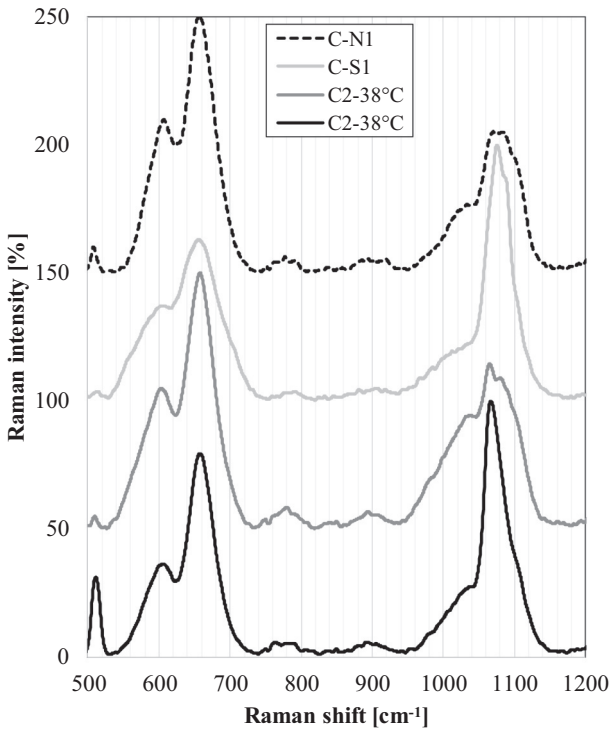

Fig. 8. Raman spectra of amorphous ASR products formed in aggregates of concrete C2–38, C-S1 and C-N1. Element ratios are given in Table 1.

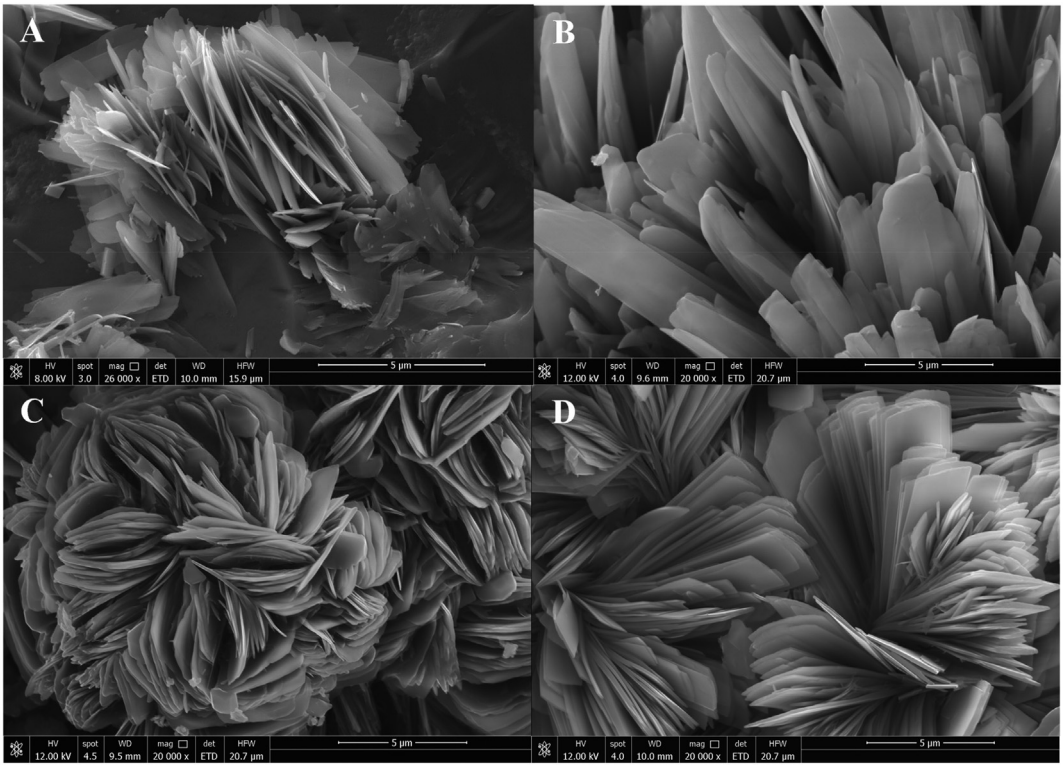

Fig. 7. Crystalline ASR product formed in aggregate particles: concrete of a bridge (A), concrete C1–60 (B), C2–38 (C) and C2–60 (D). HFW = 15.9 µm (A) and 20.7 µm (B, C, D).

Table 5
Position and relative intensity of the Raman bands of the amorphous ASR products formed in concrete aggregates and of synthetic ASR products with different Ca/Si-ratios.

C2–38	C2–38	C-N1	C-S1	Syn-0.07	Syn-0.17	Syn-0.27	Syn-0.33
[cm^{-1}]							
1080 (60)	1078 (100)	1077 (56)	1076 (100)	1079 (92)	1080 (97)	1080 (88)	1079 (75)
–	–	–	–	910 (19)	911 (15)	924 (20)	930 (34)
–	–	–	–	779 (9)	779 (8)	778 (5)	778 (5)
658 (100)	658 (79)	657 (100)	656 (64)	652 (64)	652 (100)	651 (100)	650 (100)
604 (56)	606 (37)	607 (61)	606 (38)	571 (100)	597 (98)	606 (74)	606 (59)

to avoid the impact of calcium uptake from the cement paste on the ASR products in the post-cracking state, which can reach a depth of up to 30 μm.

The Raman spectra of the amorphous products display always the same pattern. In the range of the bending vibrations there are two distinct bands at ~600 cm^{-1} and another stronger one at ~650 cm^{-1} (Fig. 8). The first band is clearly attributable to Q^3-sites and the second one to Q^2-sites. The exact band positions and intensities of the spectra shown in Fig. 8 are given in Table 5. There is a weak band at ~790 cm^{-1} that is not attributable. The weak band at ~900 cm^{-1} is likely caused by Q_1-sites. The major band in the stretching vibration range is located at ~1080 cm^{-1} and is typical for Q_3-sites. The hump in the incline of this band at 1020–1030 cm^{-1} must be caused by Q_2-sites, but its intensity is too low to create a distinct band. The Raman spectra collected from concrete C-S1 and C-N1 display exactly the same characteristics (Fig. 8). The various bands below 550 cm^{-1} present in all samples are caused by the presence of different silicates on which the amorphous ASR products were deposited in the studied aggregates.

In order to provide a link between Raman spectra and chemical composition, EDS analysis was performed on the same locations from which the spectra in Fig. 8 were collected. However, as surface inclination and roughness may influence the EDS analysis, the determined compositions have to be regarded as indicative and are therefore only given as ratios (Table 3). However, these determined values match the ones measured on polished samples very well (Tables 3 and 4). Only in the case of concrete C-S1, an unusually high Na/K-ratio is observed.

3.1.4.2. Crystalline ASR products. The Raman spectra obtained from the crystalline ASR products in aggregates of concrete C1–60 are identical to the ones in concrete C2–60 (Fig. 9, Table 6) and both resemble the Raman spectra of K-shlykovite [13]. However, they are different from the spectra obtained in concrete C2–38. While the intense band of Si-O-Si bending vibrations attributable to Q_3-sites at about 600 cm^{-1} (Si-tetrahedra with three bridging oxygen atoms corresponding to sheets/layers) is nearly at the same position in the studied concrete mixtures tested at 38 and 60 °C, the band of Q_3-sites in the Si-O-Si stretching vibration range differs substantially. In concrete C2–60 it is located at 1087 cm^{-1} with a relative intensity of 32%, while it is located at 1110 cm^{-1} with a relative intensity of 100% in concrete C2–38. The band located between 1021 and 1026 cm^{-1} is attributable to Si-O-Si stretching vibration of Q_2-sites (Si-tetrahedra with two bridging oxygen atoms corresponding to a chain structure) and is very similar in all concrete mixtures. The Raman spectra of the crystalline ASR products in concrete C2–38 are identical to the ones obtained in concrete from civil engineering structures [15,16] and to ASR product synthesized at 40 °C [14].

3.2. Synthesized amorphous ASR products

3.2.1. Raman microscopy

The Raman spectra of the synthesized amorphous ASR products show a characteristic trend with increasing Ca/Si-ratio. In the bending

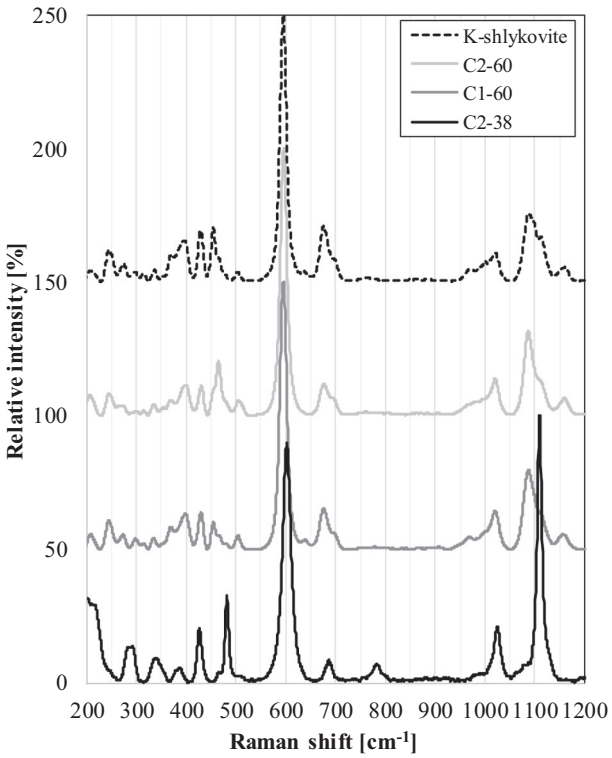

Fig. 9. Raman spectra of crystalline ASR products formed in aggregate particles concrete C1 and C2 tested at 38 and 60 °C. Spectrum of K-shlykovite from Ref. [13], see Section 3.1.4.2.

Table 6
Position and relative intensity of the Raman bands obtained from the two different types of crystalline ASR products formed in the CPT at 38 and 60 °C. Spectrum "Ref" obtained in a concrete from a bridge [16]. Spectrum "40 °C product" from crystalline product synthesized at 40 °C [14] and spectrum "K-shlykovite" from product synthesized at 80 °C [13].

C2–38	Ref	"40 °C product"	C1–60	C2–60	K-shlykovite
[cm^{-1}]			[cm^{-1}]		
1110 (100)	1110 (100)	1110 (80)	–	–	–
–	–	1087 (17)	1087 (30)	1087 (32)	1088 (26)
1025 (26)	1025 (23)	1021 (13)	1020 (15)	1020 (14)	1020 (11)
783 (7)	783 (6)	782 (7)			
687 (8)	688 (7)	677 (12)	676 (15)	676 (12)	676 (21)
602 (93)	602 (90)	603 (100)	596 (100)	596 (100)	–
–	–	–	596 (100)	596 (100)	595 (100)

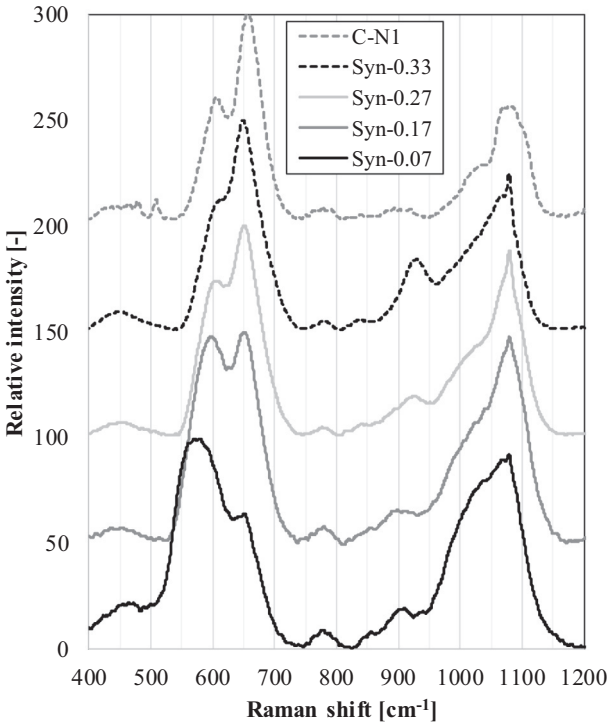

Fig. 10. Raman spectra of the synthesized amorphous ASR products and a spectrum of concrete C-N1 for comparison.

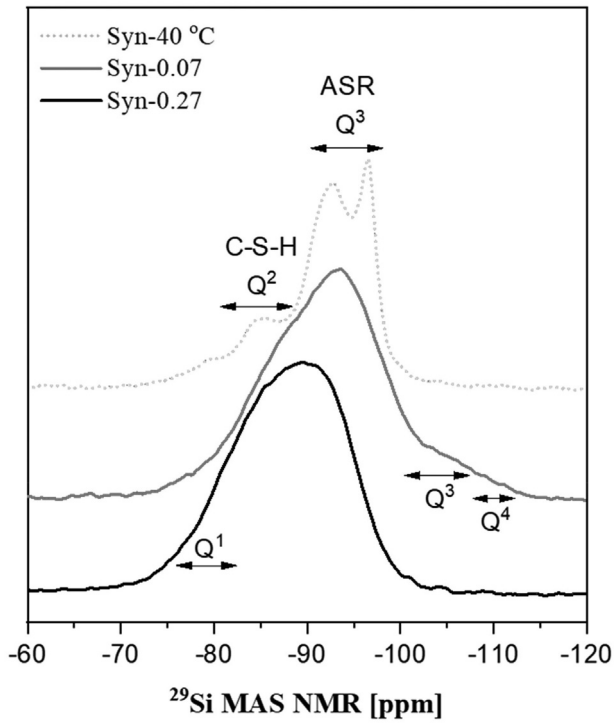

Fig. 11. ^{29}Si MAS NMR spectra of synthetic amorphous ASR products. The data for Syn-40 °C (crystalline ASR product synthesized at 40 °C) is reproduced from a previous study [14].

vibration range, the dominant band at 571 cm^{-1} and the less intense band at 652 cm^{-1} change their relative intensities with increasing Ca/Si-ratio from 0.07 to 0.33 (Fig. 10). At a Ca/Si-ratio of 0.17, their intensity is about equal, while at higher Ca/Si-ratio the band at 650 cm^{-1} becomes dominant. Moreover, there is an increase in Raman shift of the lower band from 570 to 600 cm^{-1}: The band with the lower value can be assigned to Q^3-sites and the band at 650 cm^{-1} to Q^2-sites. A non-attributable band with low intensity is present at 790 cm^{-1}. The weak band in the stretching vibration range at 900 cm^{-1} present in samples Syn-0.07 and Syn-0.17 displays an increasing intensity and a shift to higher values going to sample Syn-0.33. It is in the typical range of Q^1-sites. The dominant band in the stretching vibration range is located at 1080 cm^{-1} with a hump in the incline at 1020–1040 cm^{-1}. The first is assignable to Q^3-sites and the hump to Q^2-sites.

3.2.2. NMR

The ^{29}Si MAS NMR spectra of two selected synthetic amorphous ASR products are shown in Fig. 11. The spectrum of a crystalline ASR product synthesized at 40 °C (same to that formed in C2–38) from the previous study is used as reference for identification of different types of Si-tetrahedra in ASR products [14]. In contrast to the ^{29}Si NMR spectrum of the crystalline ASR product, which is dominated by Q^3-site of different Si-tetrahedra around −92.5 ppm and −96.5 ppm, the spectra of the amorphous ASR products are dominated by both Q^3 and Q^2-sites. Their relative intensity differs depending on the Ca/Si ratio of the reaction products, where the higher Ca/Si ratio for the sample Syn-0.27 leads to higher intensity of Q^2-sites. In addition to Q^2 and Q^3-sites, a trace of Q^1-site is also observed for the Syn-0.27, which is in line with the Raman spectra of the Ca-rich samples as shown in Fig. 10. Some more polymerized Q^3 site (around −105 ppm) and traces of Q^4-sites are observed for the Syn-0.07 sample, which indicate that the reaction of amorphous silica is incomplete due to the extremely low amount of calcium.

4. Discussion

4.1. Chemical composition

The main difference between the amorphous and the crystalline ASR products is their Na/K-ratio with higher values for the amorphous product. The ratio in the amorphous products varies between 0.46 (C1–38) to 0.76 (C1–60) with an average for the four concrete mixtures of 0.64. This is slightly above the Na/K-ratio of the cement, which is 0.57. The Na/K-ratio in the pore solution of mortars containing reactive aggregates changes during the first weeks of hydration: it increases with increasing hydration time [33–35]. After 12 weeks it reaches a value that roughly corresponds to the Na/K-ratio of the cement and stays approximately stable at least until 20 weeks. As the amorphous products form first and already cause expansion in the concrete prism test after a few weeks, there seems to be a preference for binding sodium over potassium. A possible explanation for this preference is the sol-gel process. The alkali and hydroxide ions cause the dissolution of SiO_2 in the aggregate. The tendency of the sol to precipitate depends on whether the solution is oversaturated with respect to the solid. The saturation index of alkali-silicates strongly depends on the concentration of calcium [36–38]. Calcium diffuses into the aggregate leading to supersaturation and the formation of ASR products. The gelation time of a sodium-silicate sol in the presence of calcium is faster than the one of a potassium-silicate sol [39]. Consequently, a preference for the binding of sodium can result. This is confirmed by the Na/K-ratio of the synthesized gels (Table 3). Although, Na/K-ratio of the solution was 1.0, sodium concentration in the gels is higher compared to potassium.

The Na/K-ratio of the crystalline ASR products on the other hand displays a lower value than the one of the cement, indicating a preference for potassium binding. Here, the experience of synthesizing crystalline ASR products is helpful. In the synthesis at 80 °C only the use of NaOH, KOH and a mixture of NaOH/KOH with a molar ratio of 0.16 resulted in the formation of pure Na- or K-shlykovite after a storage of 80 days [13]. Using different NaOH/KOH-ratio lead to the formation of

amorphous products only. In a parallel study to this one, the immersion of concrete sample into 1 M solutions of NaOH, KOH and KOH/NaOH (molar ratio of 1.0) at 80 °C resulted in the formation of either Na- or K-shlykovite but no intermediate composition [40]. In the synthesis at 40 °C, only the pure potassium system resulted in the formation of crystalline ASR products after a storage time between 160 and 210 days [14]. This indicates that the formation kinetics of crystalline ASR products are faster in either pure Na- or K-systems and crystalline ASR products are formed faster in the K-system at least at 40 °C. This could be a possible explanation for a higher potassium content in the crystalline ASR products than would be expected from cement composition.

There is a certain variation in the composition of crystalline ASR products formed in different aggregate particles of concrete C1–38 and C2–38, but the compositions are very close. Possible causes of the observed differences may be attributable to alkali leaching from feldspars present in the aggregate particles. ASR products formed in concrete C1–60 and C2–60 display a slightly higher average alkali content than their counterparts tested at 38 °C ((Na + K)/Si-ratio of 0.24 to 0.21 in both concrete mixtures). This seems to be reasonable, as K and Na concentration in the pore solution increase with increasing temperature, both in pure PC systems and systems blended with fly ash [41,42] and the composition of the pore solution affects the composition of ASR products [33,35]. As Ca concentration in the pore solution decreases with increasing alkali concentration, the lower Ca/Si-ratio of the ASR products formed at the 60 °C could be attributable to this effect. However, both the differences in composition from aggregate to aggregate and the difference between the composition at 38 and 60 °C are well within the variability of single point measurements, as indicated by the bars in Figs. 4 and 5.

The composition of the ASR products as determined is in line with other studies where a comparable approach of analysis was chosen [3–7,11,16,35]. This applies to ASR products formed in aggregates of both concrete structures and laboratory concrete tested with the CPT.

4.2. Raman microscopy and NMR

The analysed amorphous ASR products in the concrete mixtures are located at a distance to the ITZ ≥ 100 μm (Table 3). Moreover, their chemical composition is in line with the one of the amorphous ASR products formed further in the interior of aggregates (Table 3, Figs. 2 and 3). As such, the Raman spectra of the amorphous ASR products and the deduction in regard to their structure can be regarded as representative for the initial products formed, which lead to the cracking of aggregates and the initiation of concrete damage.

The amorphous ASR products result in broader Raman bands compared to the crystalline ASR products, indicating a less well-defined structure. In spite of this, the Raman spectra clearly indicate a similarity between these two types of products. Spectra from both are dominated by bands attributable to Q^2- and Q^3-sites. However, the relative intensities in the bending vibration range differ significantly. At a similar Ca/Si-ratio the amorphous ASR products show an intense band of Q^2-sites (656–658 cm^{-1}) and a slightly weaker band of Q^3-sites (604–607 cm^{-1}). In the crystalline product, the relative intensities are inverse with the band of Q^3-sites one order of magnitude more intense than band of Q^2-sites. However, the relative intensities of the bands attributable to Q^2- and Q^3-sites in the stretching vibration range seem to be similar in both types of products, although the band of the Q^2-sites in the case of the amorphous product is present as hump only (Fig. 10).

The location of the bands in the amorphous ASR products and their assignments are in agreement with the data of synthesized ASR products with comparable Ca/Si-ratio published in Ref. [32]. Although the Raman spectra are very similar to some published in Ref. [20], no direct relation can be made to the specific chemical composition at the location of spectra acquisition, as these data are not provided.

The analysis of the synthesized amorphous ASR products with ^{29}Si MAS NMR (Fig. 11) confirms the designation of the Raman bands to Q^2- and Q^3-sites (Fig. 10). Both Raman spectra and ^{29}Si NMR spectra show reduced intensity of Q^3-site and increased intensity of Q^2-site with increasing the calcium content of the samples. Moreover, the results in Fig. 10 show that the Raman spectra of the amorphous ASR product formed in concrete C-N1 is more similar to the spectrum of the Syn-0.27. At the same time, ^{29}Si NMR spectra indicate that Syn-0.27 is most likely not a pure phase, instead it is mixture of Q^3-dominated ASR product and Q^2-dominated C-S-H phase. Comparison of the ^{29}Si NMR spectra between Syn-0.07 and Syn-0.27 helps to reveal the reaction sequence of ASR: amorphous silica is first dissolved by the alkaline solution and subsequently depolymerized from Q^4 (−110 ppm) to Q^3 (−105 ppm)-sites of Si-tetrahedra. In presence of calcium, this preliminary Q^3-site is further depolymerized to form amorphous ASR product, which is dominated by Q^3-site with less chemical shielding (−93.5 ppm). Such depolymerization occurs further in presence of excess amount of Ca followed by formation of C-S-H. This explains very well the observation that the Ca/Si ratio of the amorphous ASR products is more scattered than that of crystalline ASR product formed in concrete samples as shown in Figs. 2 and 3. The conversion of amorphous silica to ASR products and further to C-S-H with increasing Ca content was also confirmed by thermodynamic modelling in a recent study [38].

Amorphous ASR products are clearly different to C-S-H as a comparison with published Raman spectra of C-S-H shows [13,28]. C-S-H contains no band attributable to Q^3-sites in the bending vibration range and only a minor such band in the stretching vibration range. The bands attributable to Q^2-sites dominate the Raman spectra. Still, the increasing relative intensity of the band attributable to Q^2-sites (bending vibration range) with increasing Ca/Si-ratio of the synthesized ASR products and its shift to higher wave numbers indicates a certain similarity of the amorphous ASR product to C-S-H. Such a shift can be seen as well in the amorphous ASR product extruded into the cement paste [16]. This is also observable in synthetic systems where ASR products were transformed to C-S-H at high Ca/Si ratio [33]. Moreover, micro X-ray absorption spectroscopy indicates a comparable chemical environment of calcium and potassium in both amorphous ASR products and C-S-H with a Ca/Si between 0.35 and 0.60 [12].

Although the composition of ASR products formed at 38 and 60 °C is very similar, Raman microscopy proves that the crystalline ASR products formed at 60 °C have a different crystal structure than the ASR products formed at 38 °C. The latter are identical to the ones formed in concrete structures [16] and similar to the ones of ASR products synthesized at 40 °C [14]. The ASR products formed in the concrete prism test at 60 °C on the other hand are nearly identical to the K-shlykovite synthesized at 80 °C [13]. This dependence of the type of crystalline ASR products on temperature has already been described for concrete produced with different aggregates [15] and for ASR products synthesized at different temperatures [13,14]. However, here the same concrete mix designs have been used at 38 °C and 60 °C, indicating that the aggregate type has no influence and confirming recent findings [15,24]. Therefore, the type of product formed is clearly an effect of temperature. In general, the temperature of concrete in structures is not expected to exceed 60 °C. However, when exposed to intense solar radiation in warm climates, concrete temperature close to the surface can reach up to 60 °C [43–45]. As a result, shlykovite may form in concrete exposed to such conditions. This is confirmed in concrete cubes exposed to natural conditions in Valencia on a roof top, where K-shlykovite has been identified [24]. However, it is present in minor quantities only and the majority of the crystalline product formed corresponds to the one formed in concrete structures and the concrete prism test at 38 °C.

Raman spectra, ^{29}Si NMR and powder X-ray diffraction reveals that crystalline ASR products formed in aggregates of concrete structures and shlykovite show a strong similarity between the basic structural units, but differ in the stacking behavior of these units [12,13]. Nevertheless, The ^{29}Si MAS NMR of crystalline ASR products synthesized at 40 and 80 °C show that the crystalline ASR product is a layer

silicate dominated by Si-tetrahedra with three bridging oxygen atoms (Q_3-sites) and some additional SiO_2-tetrahedra with two bridging oxygen (Q^2-sites) [13,14]. As such, these data confirm the designation of the Raman bands shown in Fig. 9.

It is often proposed that crystalline ASR products are the result of an aging process leading to the transformation of amorphous ASR products into crystalline ones [3,5,10,46]. This is obviously the case in the synthesis of bulk samples that start with the immediate formation of amorphous ASR products and their transformation into crystalline products at a later stage [13,14]. In concrete aggregates, the chronology is the same with amorphous ASR products forming prior to crystalline ones. However, there is a clear indication that crystalline ASR products can form directly without an amorphous precursor at a later stage of ASR. At the front line of the crystalline ASR products advancing towards the interior of aggregates, amorphous products are absent. This observation suggest that formation of the crystalline ASR products is related to age or stage of ASR, but it is not necessarily a result of the transformation from the amorphous ones.

5. Conclusions

The allocation of amorphous and crystalline ASR products formed in two concrete mixtures both tested with the concrete prism test at 38 and 60 °C was studied. Their chemical composition was measured and Raman spectra were acquired. Additionally, Raman and ^{29}Si MAS NMR spectra of synthesized amorphous ASR products were analysed by Raman microscopy and NMR. Based on the results, the following conclusions can be drawn:

- The microstructural evidence shows that the amorphous ASR products are the type of product formed first, which leads to the cracking of aggregates. After cracking, the crystalline ASR products start to form and fill the open cracks in the aggregates.
- The average Ca/Si-ratio of amorphous and crystalline ASR products is very similar, with values of 0.21–0.23 and 0.22–0.26, respectively. The (Na + K)/Si-ratio varies more, with values for both types of products of 0.21–0.24 and 0.22–0.34, respectively. The main difference in chemical composition concerns the Na/K-ratio, with higher values for the amorphous (0.46–0.76) compared to the crystalline ones (0.10–0.27).
- The composition of the crystalline ASR products shows little variation from aggregate to aggregate of the same concrete.
- The structure of amorphous ASR products consists mainly of Q^3-sites (Si-tetrahedra with three bridging oxygen atoms typical for a layer structure) with a secondary amount of Q^2-sites (Si-tetrahedra with two bridging oxygen atoms typical for a chain structure) as shown by Raman microscopy and ^{29}Si MAS NMR. The amount of Q^2-sites increases with increasing Ca/Si-ratio.
- Similar to the amorphous ASR product, the crystalline one is dominated by Q^3-sites with a smaller share of Q^2-sites as shown by the distinct Raman bands.
- The Raman spectra of crystalline ASR product formed in the concrete tested at 38 °C agrees with the of crystalline ASR product formed in concrete of civil engineering structures.
- The structure of the crystalline ASR product formed in the concrete tested at 60 °C is different to the one formed at 38 °C. The Raman spectrum corresponds to the one of synthesized K-shlykovite.

CRediT authorship contribution statement

Andreas Leemann: Conceptualization, Methodology, Validation, Formal analysis, Investigation, Writing - original draft, Writing - review & editing, Visualization. **Zhenguo Shi**: Methodology, Validation, Formal analysis, Investigation, Writing - review & editing. **Jan Lindgård**: Methodology, Formal analysis, Investigation, Writing - review & editing.

Declaration of competing interest

The authors declare that they have no known competing financial interests or personal relationships that could have appeared to influence the work reported in this paper.

Acknowledgements

The authors would like to thank SNF Sinergia: Alkali-silica reaction in concrete (ASR), grant number CRSII5_17108. The NMR hardware was partially granted by the Swiss National Science Foundation (SNSF, grant no. 206021_150638/1). Daniel Rentsch is acknowledged for acquiring the ^{29}Si MAS NMR spectra. The authors would like to thank A. M. López-Buendía (Aidico), P. Martí Martí (Aidico), E. Menéndez (Eduardo Torroja Institute), A. Santos Silva (LNEC) and J. Custódio (LNEC) for providing the sample exposed to outdoor conditions. P. Lura is acknowledged for the review of the manuscript.

References

[1] H. De Mayo Bernardes, N.P. Hasparyk (Eds.), Proceeding of the 15th ICAAR, Sao Paolo/Brasil, 2016.
[2] A. Leemann, B. Münch, The addition of caesium to concrete with alkali-silica reaction: implications on product identification and recognition of the reaction sequence, Cem. Concr. Res. 120 (2019) 27–35.
[3] N. Thaulow, U. Hjorth Jakobsen, B. Clark, Composition of alkali-silica gel and ettringite in concrete railroad ties: SEM-EDX and X-ray diffraction analyses, Cem. Concr. Res. 26 (1996) 309–318.
[4] I. Fernandes, Composition of alkali-silica reaction products at different locations within concrete structures, Mater. Charact. 60 (2009) 655–668.
[5] T. Katayama, ASR gels and their crystalline phases in concrete - universal products in alkali–silica, alkali–silicate and alkali–carbonate reactions, in: T. Drimalas, J.H. Ideker, B. Fournier (Eds.), Proceedings of the 14th ICAAR, Austin, Texas, 2012.
[6] A. Leemann, P. Lura, E-modulus of the alkali–silica-reaction product determined by micro-indentation, Constr. Build. Mater. 44 (2013) 221–227.
[7] A. Leemann, C. Merz, An attempt to validate the ultra-accelerated microbar and the concrete performance test with the degree of AAR-induced damage observed in concrete structures, Cem. Concr. Res. 49 (2013) 29–37.
[8] W.F. Cole, C.J. Lancucki, Products formed in an aged concrete the occurrence of okenite, Cem. Concr. Res. 13 (1983) 611–618.
[9] L. de Ceukelaire, The determination of the most common crystalline alkali–silica reaction product, Mater. Struct. 24 (1991) 169–171.
[10] K. Peterson, D. Gress, T. van Dam, L. Sutter, Crystallized alkali–silica gel in concrete from the late 1890s, Cem. Concr. Res. 36 (2006) 1523–1532.
[11] R. Dähn, A. Arakcheeva, P. Schaub, P. Pattison, G. Chapuis, D. Grolimund, ... A. Leemann, Application of micro X-ray diffraction to investigate the reaction products formed by the alkali–silica reaction in concrete structures, Cem. Concr. Res. 79 (2016) 49–56.
[12] G. Geng, Z. Shi, A. Leemann, C. Borca, T. Huthwelker, K. Glazyrin, ... E. Wieland, Atomistic structure of alkali-silica reaction products refined from X-ray diffraction and micro X-ray absorption data, Cem. Concr. Res. 129 (2020) 105958.
[13] Z. Shi, G. Geng, A. Leemann, B. Lothenbach, Synthesis, characterization, and water uptake property of alkali-silica reaction products, Cem. Concr. Res. 121 (2019) 58–71.
[14] Z. Shi, A. Leemann, D. Rentsch, B. Lothenbach, Synthesis of alkali-silica reaction product structurally identical to that formed in field concrete, Mater. Design 108562 (2020).
[15] A. Leemann, I. Borchers, M. Shakoorioskooie, M. Griffa, Ch. Müller, P. Lura, Microstructural analysis of ASR in concrete – accelerated testing versus natural exposure, Proceedings pro128: International Conference on Sustainable Materials, Systems and Structures (SMSS2019). Durability, Monitoring and Repair of Structures, RILEM Publications S.A.R.L, Paris, France, 2019.
[16] A. Leemann, Raman microscopy of alkali-silica reaction (ASR) products formed in concrete, Cem. Concr. Res. 102 (2017) 41–47.
[17] R.J. Kirkpatrick, A.G. Kalinichev, X. Hou, L. Struble, Experimental and molecular dynamics modeling studies of interlayer swelling: water incorporation in kanemite and ASR gel, Mater. Struct. 38 (2005) 449–458.
[18] X. Hou, R.J. Kirkpatrick, L.J. Struble, P.J. Monteiro, Structural investigations of alkali silicate gels, J. Am. Ceram. Soc. 88 (2005) 943–949.
[19] C.J. Benmore, P.J. Monteiro, The structure of alkali silicate gel by total scattering methods, Cem. Concr. Res. 40 (2010) 892–897.
[20] C.M. Strack, E. Barnes, M.A. Ramsey, R.K. Williams, K.L. Klaus, R.D. Moser, Impact of aggregate mineralogy and exposure solution on alkali-silica reaction product composition and structure within accelerated test conditions, Constr. Build. Mater. 240 (2020) 117929.
[21] Norwegian Concrete Association, NB, Alkali–Aggregate Reactions in Concrete, Test Methods and Requirements to Test Laboratories, NB Publication No. 32, (2005).
[22] P.J. Nixon, I. Sims (Eds.), RILEM Recommended Test Method: AAR-4.1 - Detection of Potential Alkali-Reactivity - 60° C Test Method for Aggregate Combinations Using

Concrete Prisms. In: RILEM Recommendations for the Prevention of Damage by Alkali-Aggregate Reactions in New Concrete Structures, Springer, Dordrecht, 2016, pp. 99–116.
[23] J. Lindgård, P.J. Nixon, I. Borchers, B. Schouenborg, B.J. Wigum, M. Haugen, U. Åkesson, The EU "PARTNER" Project - European standard tests to prevent alkali reactions in aggregates: final results and recommendations, Cem. Concr. Res. 40 (2010) 611–635.
[24] I. Fernandes, A. Leemann, B. Fournier, E. Menéndez, J. Lindgård, I. Borchers, J. Custódio, PARTNER Project post documentation study – condition assessment of field exposure site cubes (part II – results of microstructural analyses), Proceedings of the 16th ICAAR, Lisbon/Portugal, 2021.
[25] I. Borchers, J. Lindgård, J.C. Müller, Evaluation of laboratory test methods for assessing the alkali-reactivity potential of aggregates by field site tests, Proceedings of the 16th ICAAR, Lisbon, Portugal, 2021 (accepted).
[26] J. Lindgård, M.D. Thomas, E.J. Sellevold, B. Pedersen, Ö. Andiç-Çakır, H. Justnes, T.F. Rønning, Alkali–silica reaction (ASR) - performance testing: influence of specimen pretreatment, exposure conditions and prism size on alkali leaching and prism expansion, Cem. Concr. Res. 53 (2013) 68–90.
[27] P. McMillan, Structural studies of silicate glasses and melts - applications and limitations of Raman spectroscopy, Am. Miner. 69 (1984) 645–659.
[28] R.J. Kirkpatrick, J.L. Yarger, P.F. McMillan, Y. Ping, X. Cong, Raman spectroscopy of CSH, tobermorite, and jennite, Adv. Cem. Mater. 5 (1997) 93–99.
[29] P. Colomban, A. Tournié, L. Bellot-Gurlet, Raman identification of glassy silicates used in ceramics, glass and jewellery: a tentative differentiation guide, J. Raman Spectrosc. 37 (2006) 841–852.
[30] A.G. Kalampounias, IR and Raman spectroscopic studies of sol-gel derived alkaline-earth silicate glasses, Bull. Mater. Sci. 34 (2011) 299–303.
[31] L. De Ferri, D. Bersani, P. Colomban, P.P. Lottici, G. Simon, G. Vezzalini, Raman study of model glass with medieval compositions: artificial weathering and comparison with ancient samples, J. Raman Spectrosc. 43 (2012) 1817–1823.
[32] C. Balachandran, J.F. Muñoz, T. Arnold, Characterization of alkali silica reaction gels using Raman spectroscopy, Cem. Concr. Res. 92 (2017) 66–74.
[33] A. Leemann, B. Lothenbach, The influence of potassium–sodium ratio in cement on concrete expansion due to alkali-aggregate reaction, Cem. Concr. Res. 38 (2008) 1162–1168.
[34] A. Leemann, B. Lothenbach, C. Thalmann, Influence of superplasticizers on pore solution composition and on expansion of concrete due to alkali-silica reaction, Constr. Build. Mater. 25 (2011) 344–350.
[35] A. Leemann, B. Lörtscher, L. Bernard, L.G. Le Saout, B. Lothenbach, R.M. Espinosa-Marzal, Mitigation of ASR by the use of LiNO3 - characterization of the reaction products, Cem. Concr. Res. 59 (2014) 73–86.
[36] A. Leemann, G. Le Saout, F. Winnefeld, D. Rentsch, B. Lothenbach, Alkali–silica reaction: the influence of calcium on silica dissolution and the formation of reaction products, J. Am. Ceram. Soc. 94 (2011) 1243–1249.
[37] T. Kim, J. Olek, H. Jeong, Alkali–silica reaction: kinetics of chemistry of pore solution and calcium hydroxide content in cementitious system, Cem. Concr. Res. 71 (2015) 36–45.
[38] Z. Shi, B. Lothenbach, The role of calcium on the formation of alkali-silica reaction products, Cem. Concr. Res. 126 (2019) 105898.
[39] F. Gaboriaud, A. Nonat, D. Chaumont, A. Craievich, Aggregation and gel formation in basic silico-calco-alkaline solutions studied: a SAXS, SANS, and ELS study, J. Phys. Chem. B 103 (1999) 5775–5781.
[40] Z. Shi, S. Park, B. Lothenbach, A. Leemann, Formation of shlykovite and ASR-P1 in concrete under accelerated alkali-silica reaction at 60 and 80 °C, Cem. Concr. Res..
[41] B. Lothenbach, F. Winnefeld, C. Alder, E. Wieland, P. Lunk, Effect of temperature on the pore solution, microstructure and hydration products of Portland cement pastes, Cem. Concr. Res. 37 (2007) 483–491.
[42] F. Deschner, B. Lothenbach, F. Winnefeld, J. Neubauer, Effect of temperature on the hydration of Portland cement blended with siliceous fly ash, Cem. Concr. Res. 52 (2013) 169–181.
[43] A.K. Schindler, J.M. Ruiz, R.O. Rasmussen, G.K. Chang, L.G. Wathne, Concrete pavement temperature prediction and case studies with the FHWA HIPERPAV models, Cem. Concr. Comp. 26 (2004) 463–471.
[44] A. Arora, G. Sant, N. Neithalath, Numerical simulations to quantify the influence of phase change materials (PCMs) on the early-and later-age thermal response of concrete pavements, Cem. Concr. Comp. 81 (2017) 11–24.
[45] B.A. Young, G. Falzone, Z. She, A.M. Thiele, Z. Wei, N. Neithalath, G. Sant, L. Pilon, Early-age temperature evolutions in concrete pavements containing micro-encapsulated phase change materials, Constr. Build. Mat. 147 (2017) 466–477.
[46] G. Davies, R.E. Oberholster, Alkali-silica reaction products and their development, Cem. Concr. Res. 18 (1988) 621–635.